Chapter

Additive Manufacturing for Antenna Applications

Gregory Mitchell and David Turowski

Abstract

This chapter describes the results of additive manufacturing (AM) for a multi-band antenna that effectively replaces two with a single footprint. The antenna achieves distinct modes of operation by achieving flexibility between horizontal and vertical polarizations on transmit and receive at both S-band and X-band frequencies. Low dielectric constants of commercial AM materials limit current AM antenna designs. Research into the composition of high-dielectric feedstocks for AM opens the design space for 3D printed hybrid material antennas. We compare the performance of an AM antenna to the same prototype using traditional methods and materials.

Keywords: additive manufacturing, dual-band antenna, dual polarization, 3D printing

1. Introduction

Additive manufacturing (AM), also known as 3D printing, allows engineers to rethink the traditional antenna design space. AM facilitates complex designs that require properties not achievable by current manufacturing methods. The 3D and hybrid-material approaches needed to achieve these designs makes AM critical to the future of radio frequency (RF) systems.

New research is spearheading development of RF AM technology to facilitate development of scalable AM antennas with built-in frequency and polarization agility. AM is a disruptive technology that facilitates complex designs requiring properties not achievable by current manufacturing methods. Strides in AM show robust structural and mechanical parts, but industry has yet to develop and fully characterize a large suite of RF materials compatible with AM methods. Low dielectric constants of commercial feedstocks limit current AM antenna designs. Recent research into the composition of high-dielectric feedstocks and for AM opens the design space for 3D printed hybrid material antennas [1–3]. This research includes loading low-loss polymer matrices such as acrylonitrile butadiene styrene (ABS) with varying volumes of high-dielectric ceramic nanoparticles. However, increasing the volume percentage of high-dielectric ceramics creates brittle filaments, which break when spooled and bind when printing, making dielectric constants greater than 8 unviable for fused deposition modeling (FDM) printers. However, initial research into incorporating the filament extrusion step directly at the print head shows promise by eliminating the need to print from a pre-fabricated spool of filament effectively sidestepping the ceramic volume loading limitation

previously mentioned. This technique could open the doors for even higher dielectric AM filaments because designers will not need to spool or flex the highly loaded polymer in order to print with it.

Currently, AM produces robust structural and mechanical parts, but designers have yet to fully develop and characterize electromagnetic properties of AM feedstocks for printing antennas and other RF devices. Recent research into the composition of high-permittivity feedstocks for AM opens the design space for hybrid material antennas, and necessitates an emphasis on the measurement of electromagnetic properties for printed dielectric substrates.

Novel high dielectrics and conductive inks for AM enable complex and integrated antenna designs in all three dimensions. This leads to our integration of our S−/X-band antenna into a single aperture allowing for simultaneous multiband capabilities. The 3D and hybrid material approaches needed to achieve this scalable, agile, and multimode antenna demonstrate the necessity of AM for future of RF systems. Additionally, AM enables on demand supply closer to the point of need. This reduces the logistical burden, cost, and upgradeability of RF system maintenance in the field. These benefits result rapid development of new technologies, and increases agility to address new RF needs as they emerge in near real time.

This chapter focuses on the benefits and negatives of AM pertaining to antennas. AM dielectric substrates enable multiband approaches to AM phased arrays. We demonstrate our AM antenna by comparing experimental data to an identical antenna manufactured via legacy materials and techniques.

2. Role of additive manufacturing for antennas and radio frequency components

As governments, industries, and universities move toward multipurpose wireless platforms, engineers must integrate functionality of disparate frequency bands into single systems. This requires planar and vertical integration of apertures, substrates, and feed networks to enable multiple modes of operation. Now RF front ends must integrate several different antennas and their feed networks consisting of transmission lines, amplifiers, filters, and switches across increasing bandwidth. Integrated designs require both hybrid material and fully volumetric, as opposed to planar, approaches. The ability of AM to achieve geometries not possible by today's manufacturing processes makes AM a critical enabler of future of RF systems.

In the recent past, designers achieved robust mechanical and structural components through AM processes, but companies have not yet developed AM materials and feedstocks suitable for the design of antennas and other RF components. Engineers must also conduct research in the area of conductive inks for AM. Current silver inks yield metal layers with lower conductivity compared to their bulk metal counterparts. Increased conductivity of printable inks enhances the power efficiency of RF components.

Currently, low dielectric constants of commercially available AM feedstocks are limiting antenna designs. However, through the development of high-dielectric constant and low-loss electromagnetic materials, AM opens the RF design space to complex geometries and material gradients not currently achievable. One example is the Luneberg lens [1], which relies on a graded dielectric constant. By controlling the fill density of printed substrates, AM achieves a continuously graded slope in dielectric constant that is the enabling feature of the Luneberg lens design [2].

Increasing the RF versatility of AM requires research into feedstocks that achieve high dielectric constants. Recent research shows AM filaments with dielectric constants 0f 4 or greater can be extruded from polymer/ceramic

composites [3–6]. The process loads a low-loss host polymer with a given volume fraction 0f ceramic nanoparticles with high dielectric constants. The host polymer will tend to have a low dielectric constant and the volume fraction of the dispersed high-dielectric ceramic particles will determine the macroscopic dielectric constant of the extruded filament [5, 7]. Since we know the presence of voids during the 3D printing process can cause deviations in the dielectric constant, electromagnetic characterization of the final substrate becomes very important.

AM for hybrid material antennas has additional obstacles other than limitations in dielectric constant. The layered nature of 3D printing causes the potential for inconsistencies in the bonding of interfaces between printed layers. Similarly, 3D printing processes yield anisotropy in the electromagnetic properties of printed layers that can yield RF properties that differ depending on direction within the printed substrate. Porosity, surface roughness, and repetitiveness are also concerns relating to AM technologies for antennas and RF devices [8–11].

Beyond dielectric feedstocks for AM, research into increasing the conductivity of printable inks is also of interest. The best conductivity of conductive inks is currently 5–10 times less than that of bulk metals, and even these reduced conductivities require sintering processes in excess of 175°C [12]. Reduced conductivity will cause decreased radiation efficiency in antennas and increased transport inefficiencies in transmission lines. Whereas high sintering temperatures required for 3D printed inks would degrade and melt the thermoplastic-based dielectric compounds discussed previously. There are alternate methods for sintering currently under investigation such as laser sintering and flash annealing, but these methods still require further research to demonstrate their viability.

2.1 High-dielectric filaments compatible with additive manufacturing

Current research investigates methods for extruding high-dielectric AM filaments through a robust and repeatable method that allows for the printing of AM substrates with a given value of dielectric constant. This will give engineers a continuum of achievable dielectric constants for AM substrates they can use in their models when designing RF components. A second challenge is developing a technique for sintering of conductive inks printed on an AM substrate without compromising the integrity of the dielectric substrate. A final hurdle is to produce a fully integrated AM antenna including ground plane, RF connectors, feed, multiple dielectric substrates, and aperture through a fully automated process.

Typically, composite materials are prepared using mixing techniques such as dissolving pellets of ABS using acetone [12, 13]. Afterward, mixers add plasticizers and surfactants in small concentrations. These additives are necessary, as the plasticizer acts as a lubricant between molecular chains in the polymer, enabling flexibility even with loading of ceramic powders; however, the addition of too much plasticizer negatively affects the composite by rendering it too elastic. Materials use surfactants to prevent aggregation between the ceramic particles [14].

Adding high-dielectric ceramic nanoparticles in in volume fractions between 15 and 30% to the mixtures allows to them to homogenize within the polymer. Once the acetone has fully evaporated, we cut the composite slab into pieces and then ground them into approximately 2-mm pellets. We can then extrude filaments at high temperature, but this process has its limitations. Adding more than 40% by volume of ceramic powder results in a filament too brittle for use, even with the addition of plasticizer. Furthermore, as the loading of ceramic inclusions increases, so too does the viscosity of the material. Designers must exercise care, as viscous materials are prone to printing defects, such as voids [14].

3. Hybrid material dual-band and dual-polarization antenna design

As the world continues to move to fully integrated multifunction antennas, the design of new multiband and multimode antenna geometries continues to yield structures that are more complicated to manufacture. However, current challenges in maintaining, upgrading, and networking an ever-increasing number of antenna nodes are alleviated through adapting these types of multifunction antennas and other RF devices. The low profile and lightweight designs of references [15–18] show great promise for multifunction antenna applications. This chapter compares the performance of a multifunction antenna prototyped using traditional off-the-shelf materials and fabrication techniques, to the same antenna geometry manufactured using AM materials and 3D printing manufacturing processes. The idea being that the versatility allowed via AM of antennas can help navigate the newfound complexities of emerging multifunction antenna designs.

3.1 Antenna performance using conventional materials and techniques

We base the hybrid substrate-shared aperture antenna on the shorted annular ring and concentric patch geometry explored by Dorsey and Zaghloul [15–17]. **Figure 1** (left) shows the geometry of the dual-band antenna on two nested dielectric substrates, and **Figure 1** (right) shows the layout of the nested substrates themselves. **Table 1** gives the values in millimeters for the antenna dimensions illustrated in **Figure 1**. We shrink the overall footprint of the dual-band antenna by 30% by increasing the dielectric constant of the substrate under the annular ring from ε_{r1} = 2.33 to ε_{r1} = 6.15.

Two pairs of orthogonal microstrip pin feeds control the different operational modes of the antenna by exciting either S- or X-band frequencies and either vertical or horizontal polarization. **Figure 2** gives the locations of the pin feeds with respect to the annular ring and concentric patch antennas respectively. **Figure 2** also shows a shorting wall grounding the inner perimeter of the annular ring to diminish surface waves. Suppression of surface waves on the dielectric substrates helps

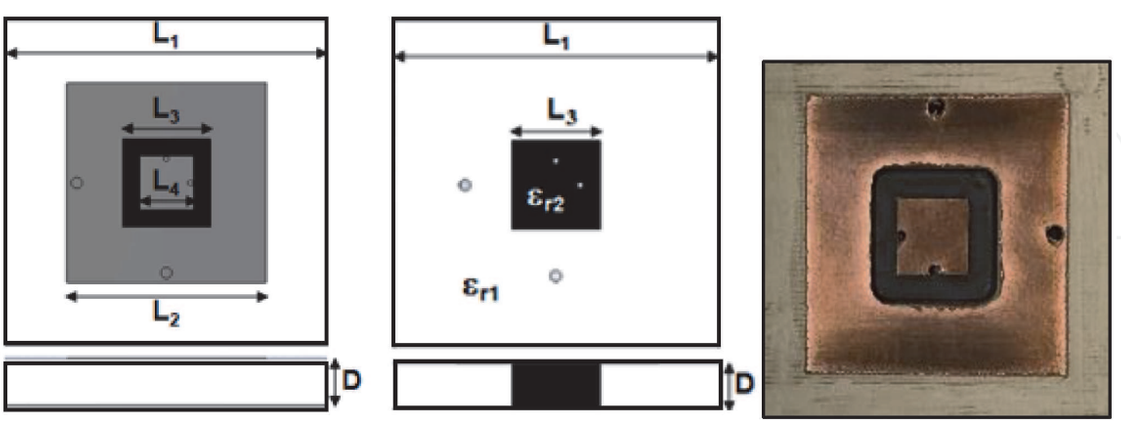

Figure 1.
Top view geometry of the dual-band antenna (left), layout of the nested substrates (center), and top view of the prototype dual-band antenna.

L_1	L_2	L_3	L_4	D	ε_{r1}	ε_{r2}
36.7	22.57	10.23	7.08	5.07	6.15	2.33

Table 1.
Antenna dimensions in millimeters of ***Figure 1****.*

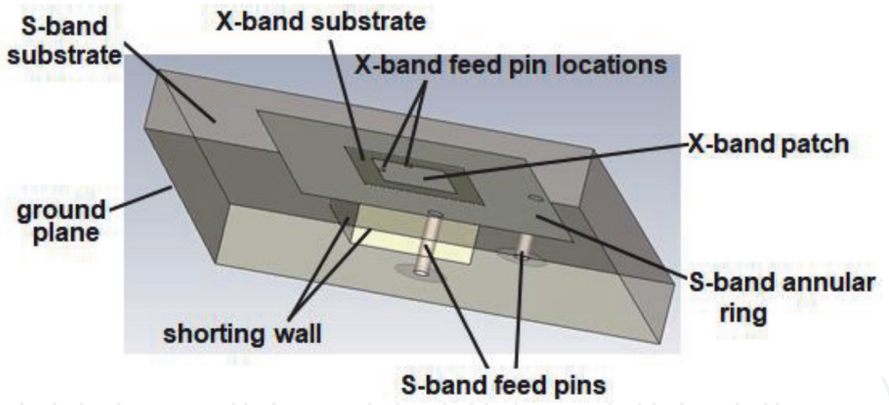

Figure 2.
3D view of the dual-band antenna and pin feed network. The outer dielectric layer is transparent for clarity.

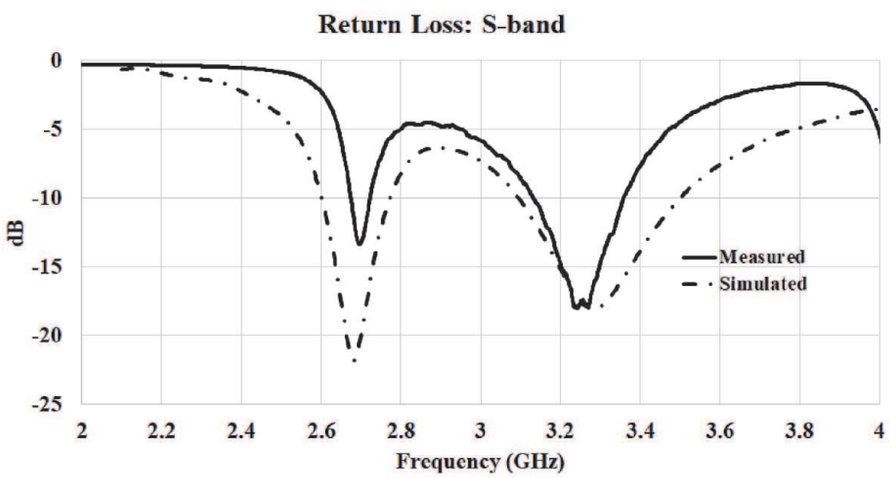

Figure 3.
Comparison of simulated return loss to measured return loss of the horizontal port at S-band.

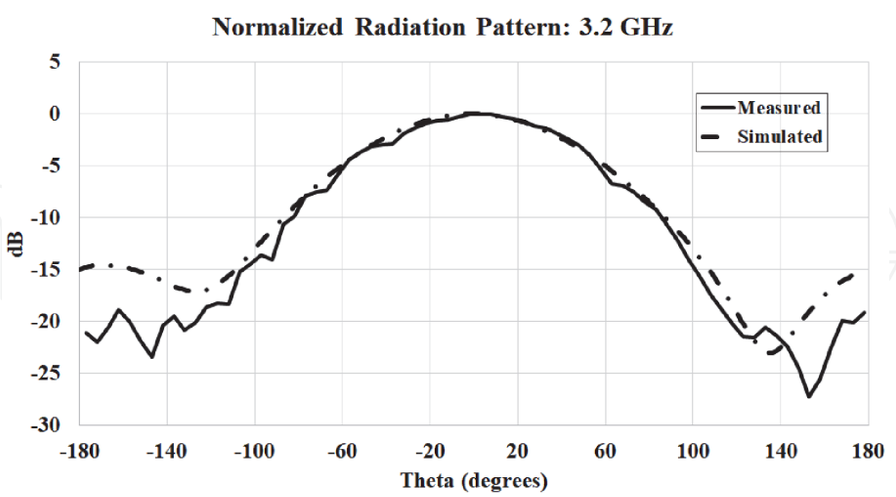

Figure 4.
Measured and simulated normalized radiation pattern at S-band horizontal port.

increases isolation between the excitation ports of the dual-band antenna. The antenna comprises a top metal layer, a hybrid Rogers 3006/Rogers 5870 substrate layer, and a bottom metal ground layer. All metal layers are 0.1 mm thick, and the dielectric substrate layer is 5.05 mm thick.

Figures 3 and **4** show the measured versus simulated return loss and normalized radiation patterns of the dual-band antenna at S-band. **Figures 5** and **6** show the

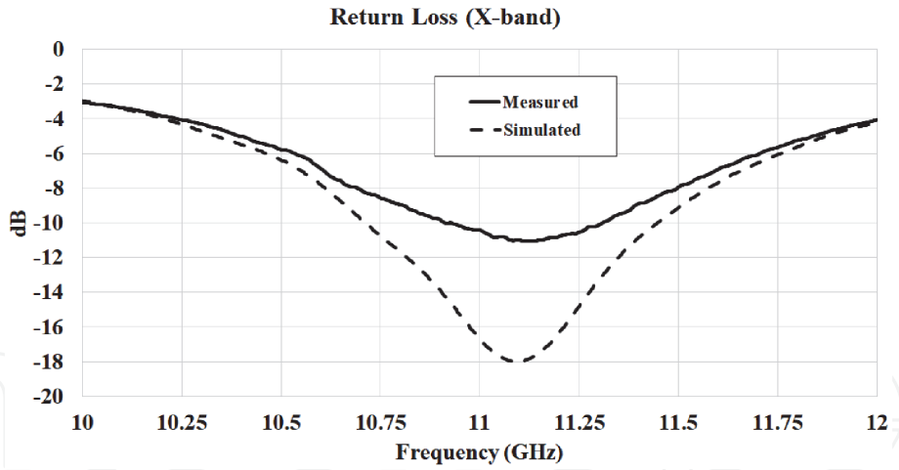

Figure 5.
Measured and simulated return loss at X-band horizontal port.

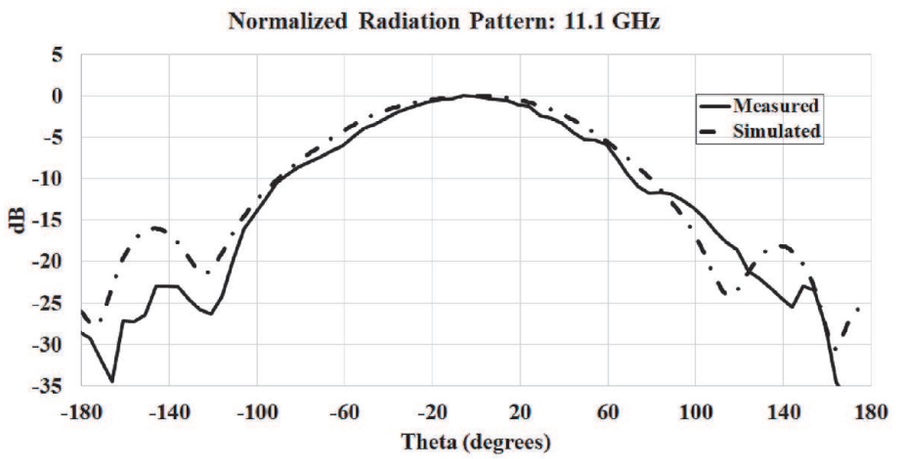

Figure 6.
Measured and simulated normalized radiation pattern at X-band horizontal port.

same for at X-band. The radiation shows good agreement at both S-band and X-band. **Figures 3** and **5** show a return loss measurement of −17.5 dB at the resonant frequency of 3.2 GHz and measurement of −11.0 dB at the resonant frequency of 11.1 GHz. There is a second S-band resonance seen at a frequency of 2.7 GHz in **Figure 3**, but the radiation characteristics in **Figure 4** show that this is not the dominant S-band resonance. We attribute discrepancies in the depth of the return loss curve in **Figure 5** to manufacturing tolerances in the placement of the pin feeds with respect to the edges of the concentric patch. Since electrical length decreases with wavelength at X-band, smaller tolerance errors can have larger effects than at S-band on the impedance match quality. However, both the simulated and measured resonant frequency at X-band is the same as expected.

3.2 Antenna performance using additive manufacturing

AM allows engineers to rethink the RF design space. AM facilitates complex designs that required properties not achievable by traditional manufacturing methods. Strides in AM produce robust structural and mechanical parts, but industry has yet to develop a full suite of electromagnetic properties for AM feedstocks. Low dielectric constants of commercial feedstocks limit current antenna designs, but recent research into the composition of high-dielectric feedstocks for AM opens the design space for antennas [12–14]. Additionally, space-filling algorithms paired

with the extrusion of high-dielectric filaments, discussed in Section 2.1, allow customized dielectric constants not previously achievable [2].

We choose a slightly modified version of the antenna design presented in Section 3.1. Due to the hybrid material design and the utilization of a fully embedded vertical shorting wall, we believe this is a good design to test capabilities of AM as it pertains to antennas. For this investigation, we design the dual-band antenna for S-band and X-band respectively. We perform all simulations using the finite difference time domain (FDTD) solver of CST Studio Suite 2019.

Figure 7 shows a to-scale 3D printed prototype of the antenna shown in **Figures 1** and **2**. The antenna utilizes a microstrip stack of a printed copper layer, hybrid dielectric layer, and a copper ground layer. We printed all pieces separately and assembled by hand afterward. All conductive layers are 1.0 mm thick. The hybrid substrate layer is 5.05 mm thick. The total profile of the antenna is 6.05 mm due to printing thicker metal layers to prevent warping.

Table 2 shows the dimensions of the geometries given in **Figure 2** as they pertain to **Figure 7**. We chose two AM filaments compatible with a Fuse Deposition Modeling (FDM) 3D printer. For the high dielectric, we chose Preperm ABS 650 with a reported dielectric constant of ε_r = 6.5 to mimic the Rogers 6010 material with ε_r = 6.15. However, after conducting waveguide measurements on a 3D printed sample, we found anisotropic values of ε_{rx} = ε_{ry} = 5.7 and ε_{rz} = 5.3. We chose ABS to mimic the Rogers 5870 material with ε_r = 2.33. Measured values of the ABS were nearly isotropic with a value of ε_r = 2.38. The loss tangents of both materials were about 10^{-3}. We printed the metal layers via the selective laser sintering (SLS) method allowing us to print actual copper as opposed to using a lower conductivity ink. Using a substrate of ε_{r1} = 5.3 instead of ε_{r1} = 6.15 under the S-band element shifts the resonances from 3.2 to 3.8 GHz. Changing the dimensions of the concentric slot and X-band patch, shown in **Figure 1** and **Table 2**, shifts the X-band frequency from 11.1 to 9.35 GHz.

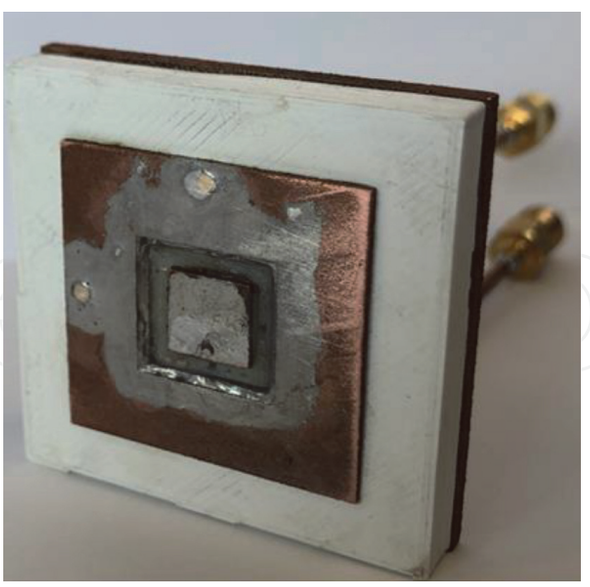

Figure 7.
Fully assembled AM dual-band antenna.

L_1	L_2	L_3	L_4	D	ε_{r1}	ε_{r2}
37.08	25.36	11.03	7.38	7.05	5.3	2.38

Table 2.
Antenna dimensions in millimeters of 3D printed antenna based on schematic in ***Figure 1****.*

We show the measured versus simulated return loss and realized gain of the dual-band antenna at S-band in **Figures 8** and **9** as well as at X-band in **Figures 10** and **11**. We took all realized gain versus frequency measurements at boresight to the antenna. We see general agreement at both bands for all measurements. One

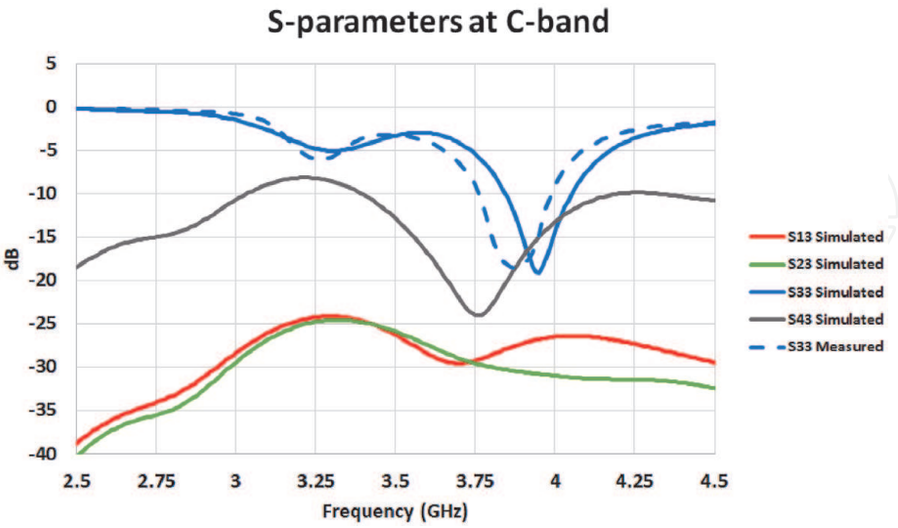

Figure 8.
S-parameters at S-band horizontal polarization port.

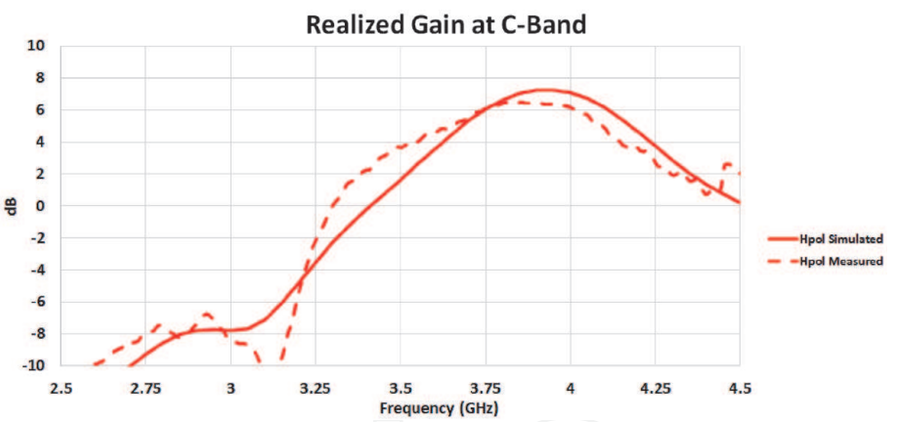

Figure 9.
Realized gain to boresight at S-band horizontal polarization port.

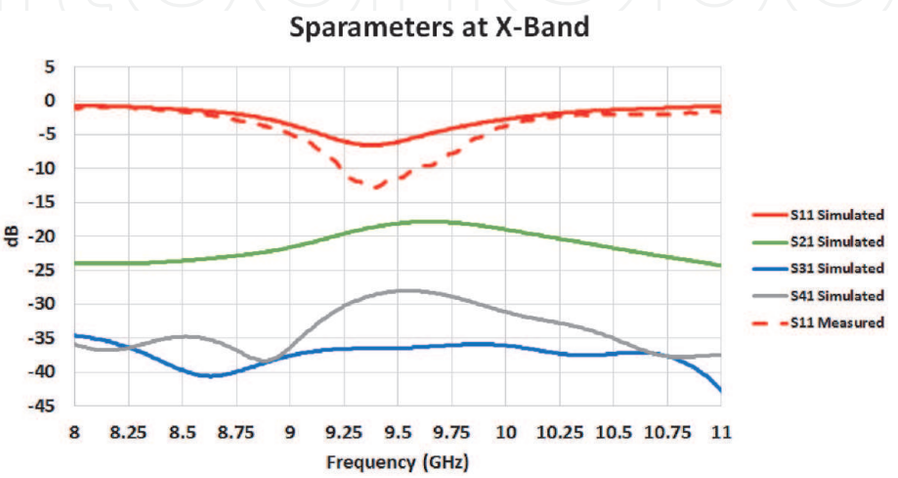

Figure 10.
S-parameters at X-band horizontal polarization port.

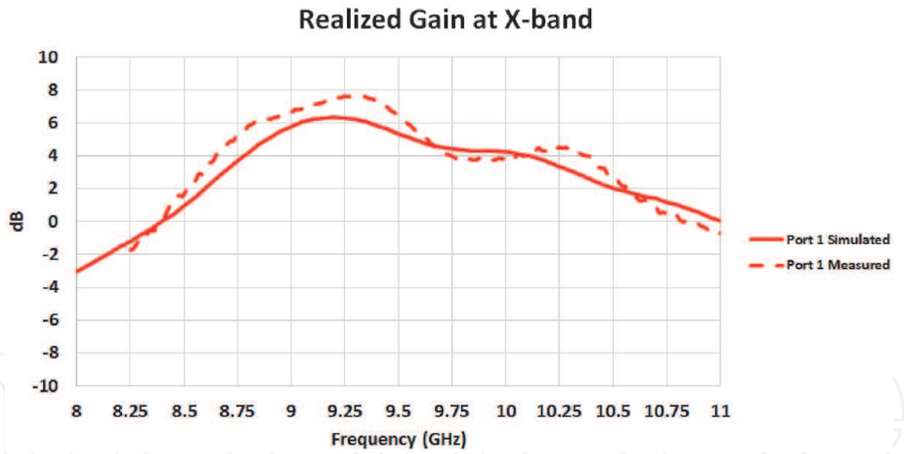

Figure 11.
Realized gain to boresight at S-band horizontal polarization port.

discrepancy is in the S-band realized gain where measurements are up to 2.0 dB lower than expected from 3.25 to 3.6 GHz. The resonance at S-band is also about 100 MHz or 2.6% off. The X-band resonance and realized gain curves show better agreement than those at S-band. The return loss at X-band is even better than that predicted by simulation and this shows up in **Figure 11** where the measured realized gain is higher than simulation at resonance.

We attribute measured differences in the return loss to manufacturing tolerances since the pin fed patch is an extremely resonant type of feed.

4. Conclusions

This chapter describes both the benefits and current challenges facing AM for antennas and RF devices. The forefront of which is a lack of commercially available high-dielectric materials that are compatible with filament fed 3D printers. As a comparison, we fabricated two similar antenna designs utilizing multiple nested dielectrics and an embedded shorting wall within the dielectrics to compare performance between traditional materials and manufacturing methods versus those of AM. Due to restricted access to an AM feedstock with the proper dielectric constant, direct comparisons of the two antennas is not the preferred way of comparison. However, experimental results for both prototypes agree well with the simulation data. There also seems to be no degradation in the performance of the AM prototype over the traditional prototype in terms of the agreement with the respective antenna models. With new methods of extruding higher dielectric filaments for FDM 3D printers, AM seems to be a good fit for future work in antenna design especially as antenna and RF front ends grow increasingly complex and more fully integrated.

Author details

Gregory Mitchell[1*] and David Turowski[2]

1 Army Research Laboratory, Adelphi, USA

2 Lockheed Martin, Moorestown, USA

*Address all correspondence to: gregory.a.mitchell1.civ@mail.mil

References

[1] Luneburg R, Herzberger M. Mint: A mathematical theory of optics. American Journal of Physics. 1996;**34** (80). DOI: 10.1119/1.1972799

[2] Roper GB, Yarlagadda S, Mirotznik M. Fabrication of a flat Luneburg lens using functional additive manufacturing. In: Proceedings of National Radio Science Meeting (Joint AP-S Symposium), USNC-URSI, Memphis, TN; 6–11 July 2014; DOI: 10.1109/USNC-URSI.2014.6955649

[3] Moulart A, Marrett C, Colton J. Mint: Polymeric composites for use in electronic and microwave devices. Journal of Polymer Engineering and Science. 2004;**44**:588-597. DOI: 10.1002/pen.20053

[4] Agarwala MK et al. Structural ceramics by fused deposition of ceramics. In: Proceedings of Solid Freeform Fabrication Symposium. Austin, TX. 1995. pp. 1-8

[5] Duncan B et al. 3D printing of millimeter wave RF devices. In: Workshop on Additive Manufacturing of Antennas and Electromagnetic Structures. McLean, VA: MITRE; 2017

[6] Castles F, et al. "Microwave Dielectric Characterization of 3D-Printed $BaTiO_3$/ABS Polymer Composities", US National Library of Medicine, PMC4778131; 2016. Available from: https://www.ncbi.nlm.nih.gov/pmc/articles/PMC4778131/#b20

[7] Rao Y et al. Novel polymer-ceramic nanocomposite based on high dielectric constant epoxy formula for embedded capacitor application. Journal of Applied Polymer Science. 28 Nov 2001;**83**(5): 1084-1090. Available from: https://doi.org/10.1002/app.10082

[8] Ahn D et al. Representation of surface roughness in fused deposition modeling. Journal of Materials Processing Technology. 2009;**209** (15-16):5593-5600

[9] Sood A et al. Improved dimensional accuracy of fused deposition modeling processed part using grey Taguchi method. Journal of Material and Design. 2009;**30**(10):4243-4252

[10] Ang K et al. Investigation of the mechanical properties and porosity relationships in fused deposition modeling-fabricated porous structures. Rapid Prototyping Journal. 2006;**12**(2): 100-105

[11] Roberson D, Wicker R, MacDonald E. Ohmic curing of printed silver conductive traces. Journal of Electronic Materials. 2012;**41**(9):2553-2566

[12] Parsons P, Larimore Z, Muhammed F, Mirotznik M. Fabrication of low dielectric constant composite filaments for use in fused filament 3D printing. Additive Manufacturing, Science Direct. December 2019;**30**. Available from: https://doi.org/10.1016/j.addma.2019.100888

[13] Castles F, Isakov D, Lui A, Lei Q, Dancer CEJ, Wang Y, et al. Microwave dielectric characterization of 3D-printed $BaTiO_3$/ABS polymer composites. Scientific Reports. 2016;**6**. Available from: https://doi.org/10.1038/srep22714

[14] Parsons P, Larimore Z, Mitchell G. Composite materials development for fused filament fabrication of RF systems. In: Proceedings of Applied Computational Electromagnetics Symposium (ACES). Monterey, CA; March 2020

[15] Dorsey W, Zaghloul A. Dual-polarized dual-band antenna element for ISM bands. In: Proceedings of IEEE

Antennas and Propagation Society. International Symposium. Charleston, SC: APS/URSI; 2009

[16] Zaghloul A, Dorsey W. Evolutionary development of a dual-band, dual-polarization, low-profile printed circuit antenna. In: Proceedings of International Conference on Electromagnetics in Advanced Applications. Torino, IT: ICEAA; 2009. pp. 994-997

[17] Dorsey W, Zaghloul A. Dual-band dual-circularly polarized antenna element. IET Microwaves, Antennas and Propagation. 2013;7:283-290

[18] Khan M, Yang Z, Warnick K. Dual-circular-polarized high-efficiency antenna for ku-band satellite communication. IEEE Antennas and Wireless Propagation Letters. 2014;**13**: 1624-1627